Ceramics International 42 (2016) 12005–12009

Contents lists available at ScienceDirect

Ceramics International

journal homepage: www.elsevier.com/locate/ceramint

Effects of LiF addition on microstructure and dielectric properties of $CaCu_3Ti_4O_{12}$ ceramics

T.C. Porfirio *, E.N.S. Muccillo

Energy and Nuclear Research Institute – IPEN, PO Box 11049, Sao Paulo, SP 05422-970, Brazil

ARTICLE INFO

Article history:
Received 19 February 2016
Received in revised form
14 April 2016
Accepted 22 April 2016
Available online 23 April 2016

Keywords:
A. Sintering
C. Dielectric properties
D. Perovskites
E. Capacitors

ABSTRACT

The effects of small amounts of lithium fluoride sintering aid on the microstructure and dielectric properties of $CaCu_3Ti_4O_{12}$ (CCTO) ceramics were investigated. CCTO polycrystalline ceramics with 0.5 and 1.0 mol% LiF, and without additive were prepared by solid state synthesis. Good densification (> 90% of the theoretical density) was obtained for all prepared materials. Specimens without the sintering aid and sintered at 1090 °C exhibit secondary phases as an outcome of the decomposition reaction. The mean grain size is controlled by the amount of LiF in specimens containing the additive. Impedance spectroscopy measurements on $CaCu_3Ti_4O_{12}$ ceramics evidence the electrically heterogeneous nature of this material consisting of semiconductor grains along with insulating grain boundaries. The activation energy for grain boundary conduction is lower for specimens prepared with the additive, and the electric permittivity reached 53,000 for 0.5 mol% LiF containing CCTO.

1. Introduction

The mixed oxide $CaCu_3Ti_4O_{12}$, CCTO, with body-centered cubic perovskite structure has drawn much attention over the last years, due to its unusually high electric permittivity ($\varepsilon' \sim 10{,}000$) [1,2]. Moreover, unlike other dielectric materials, the electric permittivity of CCTO remains unchanged over wide ranges of temperature and frequency. These characteristics turn this mixed oxide a potential candidate for technological applications in microelectronics [3,4].

Although there is no agreement on the mechanism responsible for the special dielectric properties of CCTO, several theoretical as well as experimental studies have been conducted and support a mechanism stand on extrinsic factors to explain its dielectric properties [2,5–9]. In general, those factors influencing the microstructure are claimed as significant [10,11], specially deviation of stoichiometry [12] and change of copper valence [13].

It has also been shown that dopants and sintering aids, such as P_2O_5 [14], MoO_3 [15], Te [16], $Li_2Si_2O_5$ [17], Bi [18] and lithium, barium and magnesium carbonates [19] strongly influence the crystalline structure, the microstructure and the dielectric properties of sintered CCTO.

It is common practice to sinter CCTO polycrystalline ceramics at relatively high temperatures (around 1100 °C) to obtain dense materials [1–3,8,10,11,13,16,18–20]. Reduction of the sintering temperature would be desirable for stoichiometry control allowing better reproducibility for large-scale production. Moreover, a relatively low sintering temperature could minimize the reduction reaction of Cu^{2+} to Cu^{+} during heating, and the consequent formation of Cu_2O glassy phase. The reduction reaction is known to occur mainly at the grain boundaries for temperatures of 1065 °C and above [20].

In this work, small amounts of LiF were added to CCTO, aiming to obtain high densification at lower temperatures than the usual ones, along with good dielectric properties.

2. Experimental

2.1. Sample preparation

$CaCu_3Ti_4O_{12}$ was prepared by solid-state synthesis using TiO_2 (99.5%, Alfa Aesar), CuO (99.7%, Alfa Aesar) and $CaCO_3$ (P.A., Vetec) as starting materials. Stoichiometric amounts of the reagents were wet milled in an attritor-type high-energy mill with zirconia balls (ϕ 2 mm) and isopropyl alcohol for 30 min The milled powder was dried in an oven at 60 °C for 24 h. The calcination of the powder was carried out at 900 °C for 5 h followed by deagglomeration in an agate mortar. The calcination step was repeated amounting 10 h of heat treatment. The resultant powder mixture was utilized to prepare $CaCu_3Ti_4O_{12}$ (standard composition) and with x mol% LiF (99.99%, Alfa Aesar), $x = 0.5$ and 1.

The preparation of the standard composition involved addition

* Correspondence to: Center of Materials Science and Technology, Energy and Nuclear Research Institute – IPEN, PO Box 11049, Sao Paulo, SP 05422-970, Brazil.
E-mail address: tatiane.porfirio@usp.br (T.C. Porfirio).

http://dx.doi.org/10.1016/j.ceramint.2016.04.127
0272-8842/

of 2 wt% polyvinyl alcohol (molecular weight = 100,000) as binder material. No organic binder was added during the preparation of specimens containing the sintering aid.

Cylindrical specimens were obtained by uniaxial pressing in a stainless steel die (diameter 8 mm, 2–3 mm thickness) with 55 MPa of applied pressure. The sintering temperatures varied from 1000 to 1100 °C and the sintering time was fixed at 12 h.

2.2. Sample characterization

The crystalline phases in the powder and sintered specimens were characterized by X-ray diffraction, XRD, (Bruker-AXS, D8 Advance) in the 20–80° 2θ range with 0.05° step size and 3 s counting time using Cu K_α radiation ($\lambda = 1.5405$ Å). Indexing of the diffraction patterns was performed by comparison of the experimental profiles with those of ICDD 75-1149 of CCTO. The apparent density was determined by the immersion method and compared to the theoretical density of CCTO (4.90 g cm^{-3} [21]). Microstructure characterization was carried out by field emission gun scanning electron microscopy, FEG-SEM, (FEI, Inspect F50) on polished and thermally etched surfaces of selected specimens. The mean grain size was estimated by the intercept method [22]. The electric (electrical conductivity) and dielectric (electric permittivity and dielectric loss) properties were determined by impedance spectroscopy using a low frequency analyzer (HP 4192A) in the 5 Hz to 13 MHz range with amplitude of AC signal of 100 mV, from room temperature (~25 °C) to 200 °C. Silver was used as electrode material for electrical measurements.

3. Results and discussion

3.1. Structure and microstructure

Table 1 lists relative density, ρ_r, values of CCTO determined by the immersion method. It may be noted that the standard specimens are dense regardless the sintering temperature. The sintered density of specimens with the additive also attained good densification. These materials do not contain any organic binder that enhances the green density, and promote a close contact among adjacent particles facilitating the diffusion during sintering. In this case, the densification may be attributed to the action of the sintering aid that forms a liquid phase (at approximately 1000 °C) during sintering, providing an easy path for diffusing species. Probably the amount of liquid formed when 0.5 mol% LiF is added is too small to wet all the surface of the particles in the compact, and the densification is limited. Increase of the amount of LiF to 1 mol% resulted in fairly dense specimens at relatively low temperatures.

In what follows, results obtained for specimens sintered at selected temperatures are shown: 1080 and 1090 °C for standard specimens and for CCTO with LiF, 1025 (1 mol% LiF) and 1050 °C (0.5 mol% LiF).

Table 1
Values of relative density (ρ_r) and mean grain size (G) of CCTO specimens with and without LiF sintered at several temperatures for 12 h.

Temperature (°C)	CCTO		CCTO +0.5% LiF		CCCTO+1% LiF	
	ρ_r (%)	G (μm)	ρ_r (%)	G (μm)	ρ_r (%)	G (μm)
1000	–	–	92.5	2.2	96.9	4.2
1025	–	–	90.6	2.5	95.1	3.9
1050	–	–	90.5	2.1	93.8	4.2
1070	95.5	7.9	92.2	3.2	91.0	6.8
1080	95.3	6.3	–	–	–	–
1090	96.3	10.5	–	–	–	–

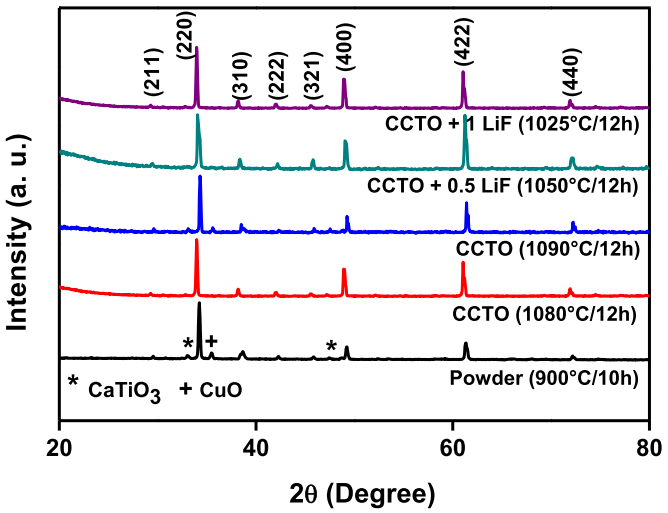

Fig. 1. Room temperature XRD patterns of the powder mixture and sintered CCTO specimens.

Fig. 1 shows XRD patterns of the calcined mixture and of CCTO sintered with and without LiF.

The XRD pattern of the calcined mixture shows the main diffraction peaks of the cubic perovskite structure of CCTO (space group *Im3*) and few diffraction peaks of secondary phases. The secondary phases were identified as $CaTiO_3$ (ICDD 39-145) and CuO (ICDD 2-1040) and are possibly a consequence of incomplete

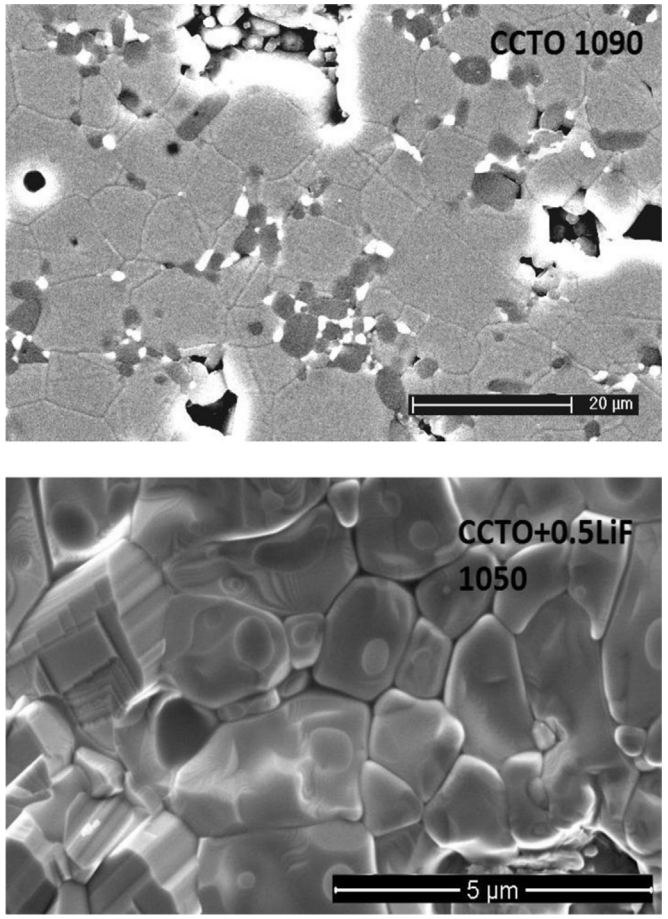

Fig. 2. FEG-SEM micrographs of CCTO sintered at 1090 °C and CCTO with 0.5 mol% LiF sintered at 1050 °C.

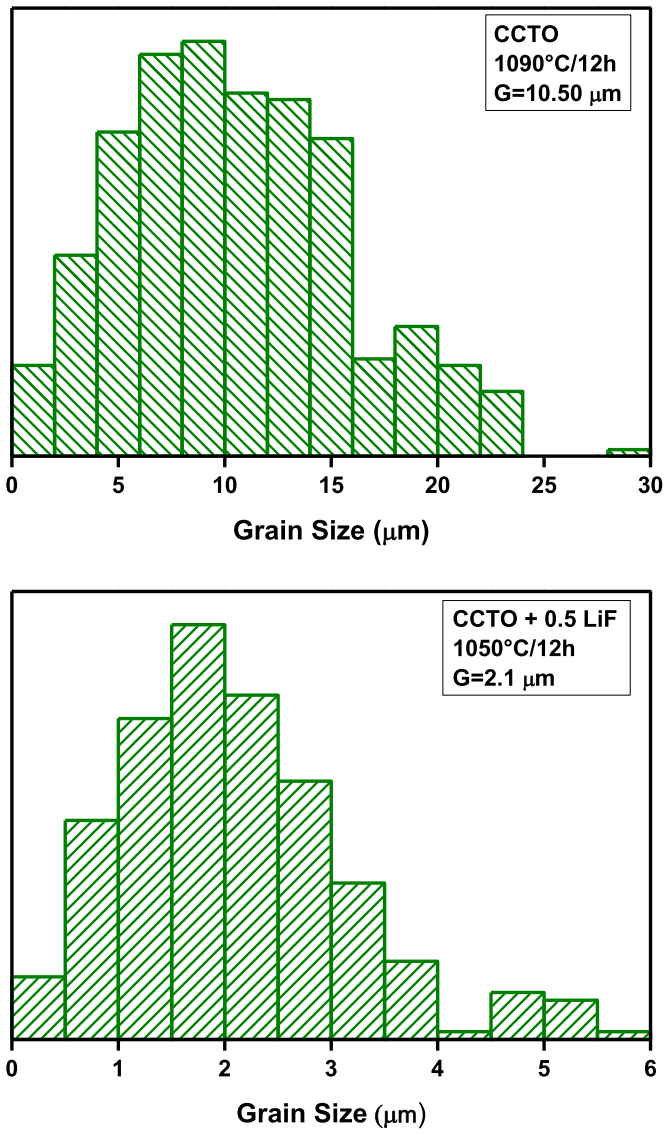

Fig. 3. Grain size distributions of selected CCTO specimens with and without LiF addition.

reaction among the starting materials at the calcination temperature. After sintering, the XRD patterns of both types of specimens, with and without LiF, exhibit only the characteristic diffraction peaks of the perovskite-type structure of CCTO, except for the standard specimen sintered at 1090 °C. The XRD pattern of the later also shows the characteristic diffraction peaks of $CaTiO_3$ and CuO secondary phases, which may be attributed, in this case, to the decomposition of CCTO, due to the relatively high sintering temperature.

Fig. 2 shows FEG-SEM typical micrographs of polished and etched surfaces of some CCTO specimens, as examples. As has been previously reported, the microstructure is heterogeneous consisting of grains with varying sizes.

The microstructure of the standard specimen sintered at 1090 °C consists of large grains with polygonal shape and small spheroidal grains. In addition porosity is detected along the grain boundaries, and grain pullout. Energy dispersive spectroscopy (EDS), analysis was carried out on this specimen to clarify the difference in the contrast of grains. The results revealed that grains with gray contrast represent the matrix with approximately 1:3:4 (Ca:Cu:Ti) stoichiometry. The fraction of Cu in dark gray grains is

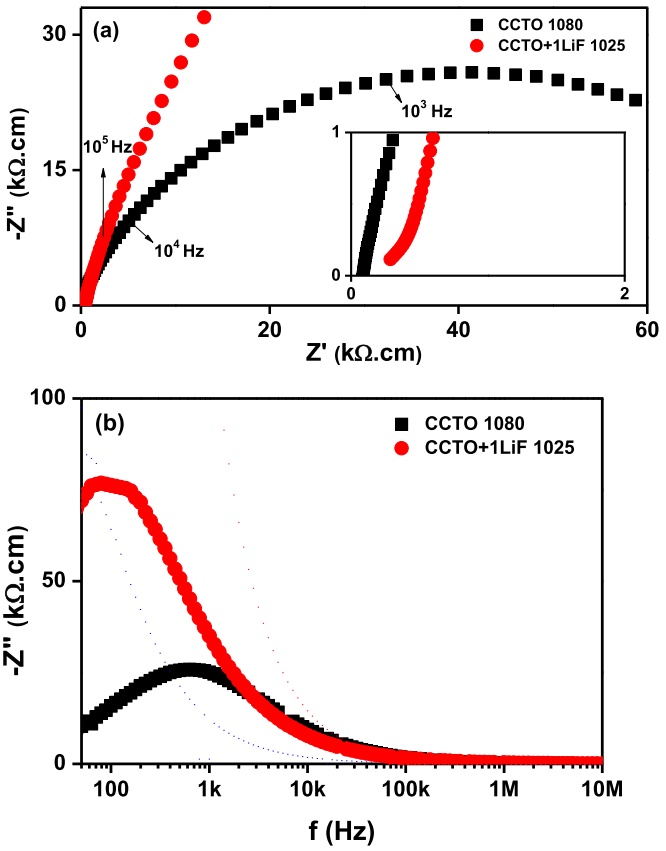

Fig. 4. (a) Impedance spectroscopy diagrams and (b) frequency dependence of the imaginary part (Z'' (ω)) of the impedance of CCTO sintered at 1080 °C, and with 1 mol% LiF sintered at 1025 °C.

very low suggesting the formation of $CaTiO_3$. It is worth noting that the diameter of the EDS probe is larger than the diameter of these small sized grains and only a qualitative determination of the elemental fractions was performed. Finally, the white contrast grains belong to a rich-Cu phase. This result agrees with XRD data (Fig. 1) and with previous observations of CCTO specimens prepared by a chemical method [23]. The morphology of CCTO with 0.5 mol% LiF exhibits more homogeneous distribution of grain sizes and no difference in contrast is observed.

The grain size distribution is shown in Fig. 3 for the same CCTO specimens.

The standard specimen sintered at high temperature possess a wide distribution of grain sizes (up to 25 μm), compared to the specimen containing LiF (up to 6 μm). Values of mean grain size estimated by the intercept method are also listed in Table 1. It may be seem that the mean grain size increases with increasing sintering temperature for CCTO specimens without the additive. For specimens containing the sintering aid, it is observed that under the same sintering conditions, such as temperature and time, it is expected that greater amounts of LiF would promote an increase of

Table 2
Values of capacitance normalized for specimen dimensions (C), activation energy for grain (E_g) and grain boundary (E_{gb}) conduction, electric permittivity (ε') and dielectric loss (tan δ) of CCTO specimens.

Specimen	E_g (eV)	E_{gb} (eV)	ε'	tan δ	C (nF cm^{-1})
CCTO 1080	0.11	0.70	26,903	1.29	2.4
CCTO 1090	0.11	0.72	14,069	0.11	1.2
CCTO+0.5% LiF 1050	0.11	0.49	53,487	0.31	9.2
CCTO+1% LiF 1025	0.11	0.31	34,994	0.68	3.0

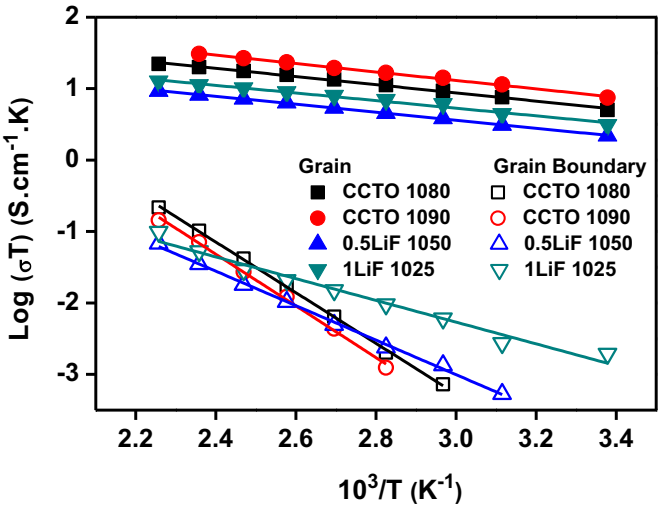

Fig. 5. Arrhenius plots of the electrical conductivity of grains and grain boundaries for CCTO with and without LiF addition.

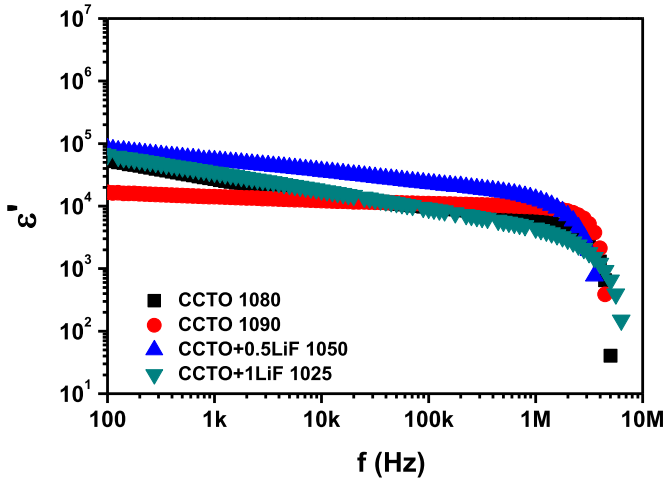

Fig. 6. Frequency dependence of the electric permittivity of sintered CCTO specimens measured at room temperature.

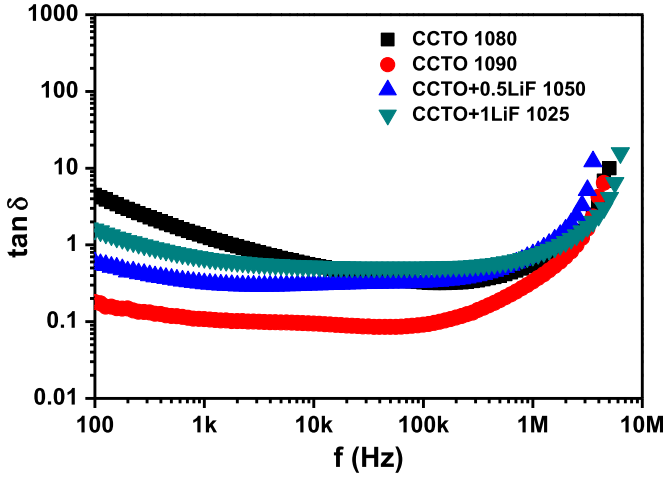

Fig. 7. Frequency dependence of the dielectric loss of sintered CCTO specimens measured at room temperature.

the glass phase at the grain boundaries, thus it would result in small average grain size. It is worthnoting that the standard CCTO specimens exhibit larger mean grain size than specimens with LiF. This effect shows that very small amounts of LiF slow down the grain growth kinetics of CCTO.

3.2. Electric and dielectric properties

Fig. 4(a) depicts room temperature $-Z''(\omega)$ versus $Z'(\omega)$ impedance plots of CCTO specimens sintered at 1080 °C and with 1 mol% LiF sintered at 1025 °C, which shows a single low frequency (< 10 kHz) semicircle. The capacitance of this semicircle is of the order of nF cm^{-1} (Table 2), in general agreement with values usually assigned to the grain boundary relaxation [24], and close to those previously reported [2]. The addition of LiF to CCTO promotes an increase of the electrical resistivity, taken at the intersection of the semicircle with the Z'-axis. The inset highlights the high frequency range of impedance, evidencing the very low grain resistivity of CCTO.

$-Z''(\omega)$ versus log (ω) plots for the same CCTO specimens are shown in Fig. 4(b). This type of representation of impedance data, the Bode diagram, emphasizes the high resistivity component, i. e., that of the grain boundaries. It may be noted that the CCTO standard specimen exhibits a maximum at ~1 kHz, whereas in the specimen with LiF the maximum amplitude of the relaxation occurs at ~0.1 kHz. This result is a consequence of changes at the grain boundaries due to LiF addition, suggesting that a fraction of the sintering aid remains at the grain boundaries after sintering.

The Arrhenius plots of the electrical conductivity of CCTO are shown in Fig. 5. The CCTO standard specimen sintered at 1090 °C exhibits the highest value of grain conductivity. All specimens display similar activation energy for grain conduction (Table 2).

The Arrhenius plots of the grain boundary conductivity of CCTO with and without LiF shown in Fig. 5 reveal a single straight line in the temperature range of measurements. However, specimens with the additive possess a different slope indicating a lower activation energy for grain boundary conduction (Table 2). This effect may be ascribed to the secondary phase formed along the grain boundaries due to the sintering aid.

Fig. 6 shows the frequency dependence of the real part of the electric permittivity measured at room temperature of CCTO with and without LiF additions. All specimens show a similar behavior with high values of ε' in a wide range of frequencies, and a sharp decrease above 1 MHz. Values of the electric permittivity at 1 kHz and room temperature are listed in Table 2. Specimens containing the additive, with lower mean grain sizes (Table 1), show higher electric permittivity values. The highest value of ε' (53,487) is found for CCTO with 0.5 mol% LiF sintered at 1050 °C, whereas the lowest value is for CCTO standard specimen sintered at 1090 °C.

The frequency dependence of the dielectric loss for sintered CCTO is shown in Fig. 7. Values of the dielectric loss determined at 1 kHz at room temperature are summarized in Table 2. The specimens of CCTO with LiF exhibit higher values of dielectric loss than to that of CCTO without LiF sintered at 1090 °C, although they are similar to those reported previously [10,14–17,20].

The overall results underline the role played by small amounts of LiF on sintering, on the final microstructure and on the electric and dielectric properties of CCTO.

4. Conclusions

Single phase polycrystalline CCTO ceramics with and without LiF addition were prepared by solid state synthesis. The formation of secondary phases is due to high sintering temperatures, as revealed by XRD experiments. Small amounts of the sintering aid are beneficial to narrow the grain size distribution, and to reduce the mean grain size. The additive allows for obtaining high densification at relatively low temperatures along with high electric

permittivity. The influence of LiF on both grain and grain boundary conductivities is evidenced by impedance spectroscopy data.

Acknowledgments

The authors acknowledge FAPESP (Proc. no. 2013/07296-2), CNPq (Proc. no. 304073/2014-8) and CNEN for financial supports. One of the authors (T.C. Porfírio) acknowledges CNPq for the scholarship.

References

[1] M.A. Subramanian, D. Li, N. Duan, B.A. Reisner, A.W. Sleight, High dielectric constant $ACu_3Ti_4O_{12}$ and $ACu_3Ti_3FeO_{12}$ phases, J. Solid State Chem. 151 (2000) 323–325, http://dx.doi.org/10.1006/jssc2000.8703.

[2] D.C. Sinclair, T.B. Adams, F.D. Morrison, A.R. West, $CaCu_3Ti_4O_{12}$: one-step internal barrier layer capacitor, Appl. Phys. Lett. 80 (2002) 2153–2155, http://dx.doi.org/10.1063/1.1463211.

[3] A.P. Ramirez, M.A. Subramanian, M. Gardel, G. Blumberg, D. Li, T. Vogt, S. M. Shapiro, Giant dielectric constant response in a copper-titanate, Solid State Comm. 115 (2000) 217–220, Doi: S0038.1098(00)00182-4.

[4] J. Li, K. Cho, N. Wu, A. Ignatiev, Correlation between dielectric properties and sintering temperatures of polycrystalline $CaCu_3Ti_4O_{12}$, IEEE Trans. Dielectr. Electr. Insul. 11 (2004) 534–541, http://dx.doi.org/10.1109/TDEI.2004.1306731.

[5] L.X. He, J.B. Neaton, M.H. Cohen, D. Vanderbilt, C.C. Homes, First-principles study of the structure and lattice dielectric response of $CaCu_3Ti_4O_{12}$, Phys. Rev. B 65 (2002) 214112, Doi: PhysRevB.65214112.

[6] M.H. Cohen, J.B. Neaton, L.X. He, D. Vanderbilt, Extrinsic models for the dielectric response of $CaCu_3Ti_4O_{12}$, J. Appl. Phys. 94 (2003) 3299–3306, http://dx.doi.org/10.1063/1.1595708.

[7] A. Tselev, C.M. Brooks, S.M. Anlage, H. Zheng, L. Salamanca-Riba, R. Ramesh, M. A. Subramanian, Evidence of power-law frequency dependence of intrinsic dielectric response in the $CaCu_3Ti_4O_{12}$, Phys. Rev. B 70 (2004) 144101, http://dx.doi.org/10.1103/PhysRevB.70.144101.

[8] R.K. Grubbs, E.L. Venturini, P.G. Clem, J.J. Richardson, B.A. Tuttle, G.A. Samara, Dielectric and magnetic properties of Fe- and Nb-doped $CaCu_3Ti_4O_{12}$, Phys. Rev. B 72 (2005) 104111, http://dx.doi.org/10.1103/PhysRevB.72.104111.

[9] S.V. Kalinin, J. Shin, G.M. Veith, A.P. Baddorf, M.V. Lobanov, H. Runge, M. Greenblatt, Real space imaging of the microscopic origins of the ultrahigh dielectric constant in polycrystalline $CaCu_3Ti_4O_{12}$, Appl. Phys. Lett. 86 (2005) 102902, http://dx.doi.org/10.1063/1.1880432.

[10] L. Marchin, S. Guillemet-Fritsch, B. Durand, A.A. Levchenko, A. Navrotsky, T. Lebey, Grain growth-controlled giant permittivity in soft chemistry $CaCu_3Ti_4O_{12}$ ceramics, J. Am. Ceram. Soc. 91 (2008) 485–489, http://dx.doi.org/10.1111/j.1551.2916.2007.02174x.

[11] R. Löhnert, R. Schmidt, J. Töpfer, Effect of sintering conditions on microstructure and dielectric properties of $CaCu_3Ti_4O_{12}$ (CCTO) ceramics, J. Electroceram. 34 (2015) 241–248, http://dx.doi.org/10.1007/s.10832-015-9982-0.

[12] S.F. Shao, J.L. Zhang, P. Zheng, C.L. Wang, Effect of Cu-stoichiometry on the dielectric and electric properties of $CaCu_3Ti_4O_{12}$ ceramics, Solid State Comm. 142 (2007) 281–286, http://dx.doi.org/10.1016/j.ssc.2007.02.025.

[13] J.F. Fernández, P. Leret, J.J. Romero, J. de Frutos, M.A. de la Rubia, M.S. Martín-Gonzalez, J.L. Costa-Kramer, J.L.G. Fierro, A. Quesada, M.A. Garcia, Proofs of the coexistence of two magnetic contributions in pure and doped $CaCu_3Ti_4O_{12}$ giant dielectric constant ceramics, J. Am. Ceram. Soc. 92 (2009) 2311–2318, http://dx.doi.org/10.1111/j.1551-2916.2009.03224x.

[14] S. Goswami, A. Sen, Low temperature sintering of CCTO using P_2O_5 as sintering aid, Ceram. Int. 36 (2010) 1629–1631, http://dx.doi.org/10.1016/j.ceramint.2010.02.036.

[15] P. Thongbai, B. Putasaeng, T. Yamwong, V. Amornkitbamrung, Liquid phase sintering behavior and improvement of giant dielectric properties by modifying microstructure and electrical response at grain boundaries of $CaCu_3Ti_{4-x}Mo_xO_{12}$ ceramics, J. Alloy. Compd. 582 (2014) 747–753, http://dx.doi.org/10.1016/j.jallcom.2013.08.119.

[16] W. Makcharoen, T. Tunkasiri, Microstructures and dielectric relaxation behaviors of pure and tellurium doped $CaCu_3Ti_4O_{12}$ ceramics prepared via vibro-milling method, Ceram. Int. 39 (2013) S359–S364, http://dx.doi.org/10.1016/j.ceramint.201210.094.

[17] T.C. Porfirio, E.N.S. Muccillo, Influence of lithium disilicate addition on the dielectric properties of chemically synthesized $CaCu_3Ti_4O_{12}$, J. Mater. Sci.: Mater. Electron. 26 (2015) 3970–3975, http://dx.doi.org/10.1007/s10854-015-2932-4.

[18] F. Luo, J. He, J. Hu, Y.-H. Lin, Electric and dielectric properties of Bi-doped $CaCu_3Ti_4O_{12}$ ceramics, J. Appl. Phys. 105 (2009) 076104, http://dx.doi.org/10.1063/1.3106054.

[19] J. Wang, L. Feng, A.L.K. Zhao, A. Yan, Preparation and dielectric properties of $CaCu_3Ti_4O_{12}$ ceramics with different additives, J. Mater. Eng. Perform. 23 (2014) 3133–3140, http://dx.doi.org/10.1007/s11665-014-1024-6.

[20] J.J. Romero, P. Leret, F. Rubio-Marcos, A. Quesada, J.F. Fernández, Evolution of the intergranular phase during sintering of $CaCu_3Ti_4O_{12}$ ceramics, J. Eur. Ceram. Soc. 30 (2010) 737–742, http://dx.doi.org/10.1016/j.jeurceramsoc.2009.08.024.

[21] T.T. Fang, C.P. Liu, Evidence of internal domains for inducing the anomalously high dielectric constant of $CaCu_3Ti_4O_{12}$, Chem. Mater. 17 (2005) 5167–5171, http://dx.doi.org/10.1021/cm051180k.

[22] M.J. Mendelson, Average grain size in polycrystalline ceramics, J. Am. Ceram. Soc. 52 (1969) 443–446, http://dx.doi.org/10.1111/j.1151-2916.1969.tb11975.x.

[23] S.K. Jo, Y.H. Han, Sintering behavior and dielectric properties of polycrystalline $CaCu_3Ti_4O_{12}$, J. Mater. Sci.: Mater. Electron. 20 (2010) 680–684, http://dx.doi.org/10.1007/s10854-008-9786-y.

[24] J.G. Fletcher, A.R. West, J.T.S. Irvine, The AC impedance response of the physical interface between yttria-stabilized zirconia and $YBa_2Cu_3O_{7-x}$, J. Electrochem. Soc. 142 (1995) 2650–2654, http://dx.doi.org/10.1149/1.2050068.